Computers and Structures 98-99 (2012) 17–22

Contents lists available at SciVerse ScienceDirect

Computers and Structures

journal homepage: www.elsevier.com/locate/compstruc

Effect of plate wave dispersion on the acoustic emission parameters in metals

D.G. Aggelis *, T.E. Matikas

Department of Materials Science and Engineering, University of Ioannina, 45110 Ioannina, Greece

ARTICLE INFO

Article history:
Received 14 September 2011
Accepted 25 January 2012
Available online 23 February 2012

Keywords:
Dispersion
Wave propagation
Numerical simulation
RA

ABSTRACT

Acoustic emission (AE) is an inspection technique for monitoring of metals. AE parameters depend on the source mechanism and proper study enlightens the material's condition. Classification criteria based on AE parameters are established concerning the material's status. However, the shape of the AE waves depends on the propagation path. Thin plates exhibit strong dispersion that influences waveform parameters. This paper numerically studies wave propagation through a homogeneous plate. The study does not concern classical parameters like velocity and attenuation, but AE waveform parameters. It is shown that any classification, should incorporate the source location in order to exclude the effect of dispersion.

1. Introduction

After the celebrated work of Kaiser [1], acoustic emission has been used for inspection of metals concerning mainly damage evaluation, or microstructural formation. Acoustic emission results from irreversible processes within the material either due to crack nucleation and propagation or changes in the microstructure. The elastic energy released on each event travels in the form of elastic waves and is captured by suitable piezoelectric sensors on the surface [2]. The number of recorded signals is correlated to the number of source incidences, while the location of the source can be estimated based on the time delay between the acquisition of each signal by different sensors [3–5]. Apart from the number of the acquired signals, qualitative parameters of the recorded waveforms shed light to the damage accumulation and mode [6–9]. Fig. 1a shows a typical AE waveform with its basic features. Indicatively, the most important parameters are the maximum amplitude (A), the duration (Dur), the number of threshold crossings (counts). Equally important features are the rise time (RT) which is the delay between the onset and the time of peak amplitude and the *RA* which is the ratio of RT/A, measured in μs/V. Energy is the area under the rectified signal envelope. Representative frequency parameters result after fast Fourier transformation, like the peak frequency, PF and the central frequency, *CF*. PF is the frequency of the maximum magnitude of the spectrum (see Fig. 1b), but it does not necessarily coincide with *CF* which is the calculated centroid of the spectrum:

$$CF = \frac{\int f \cdot M(f) df}{\int M(f) df} \quad (1)$$

where f is frequency and $M(f)$ is the fast Fourier transform (FFT) of the waveform. Another simple frequency indicator is the number of counts of the time domain waveform over its duration (average frequency, AF).

In studies related to metals, AE has been monitored during electrochemical corrosion to enhance the understanding of the phenomena occurring at aluminum or steel in electrolyte solutions [10,11]. Several of the above mentioned AE features, like peak frequency, central frequency, rise time, amplitude and energy have been correlated with irreversible processes in the material, like oxide formation or hydrogen evolution. In other cases, AE signals have been used in single fibre fragmentation tests to obtain the number of breaks and their location [12] as well as to characterize the moment of crack propagation in indentation experiments [13]. AE amplitude has been correlated to stress, in four-point bending of composite metal foam specimens [14], while the counts indicated the beginning of plastic deformation due to twinning followed by breakage of particles and decohesion between particles and the matrix in SiC reinforced alloys [15]. AE Energy and duration have been related to the failure of aluminum plates connected by a central bolt [16]. Even though the trends are not absolutely clear, the different stages of the fracture experiment, i.e. elastic deformation of the materials, slippage between the bolted plates, plasticization around the boring of the plates, and crack propagation are monitored by the change of the above mentioned AE parameters. The central frequency after wavelet transformation has been used to discern between plastic deformation and crack propagation in stainless steel coupons with notch, tested in tension [17]. Acoustic emission events and count rates have been related to crack propagation rates in steel and welded steel compact tension

* Corresponding author. Tel.: +30 26510 08006; fax: +30 26510 08054.
E-mail address: daggelis@cc.uoi.gr (D.G. Aggelis).

0045-7949/$ - see front matter © 2012 Elsevier Ltd. All rights reserved.
doi:10.1016/j.compstruc.2012.01.014

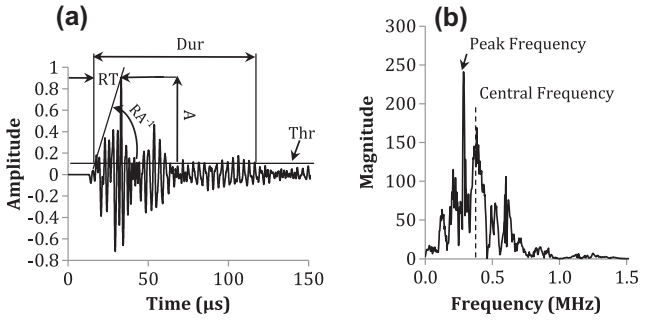

Fig. 1. (a) Typical waveform, (b) typical FFT spectrum of an AE signal.

(CT) specimens under fatigue [18]. Parameters like rise time, duration and *RA* have shown strong sensitivity to the crack propagation rate and were used to characterize the transition from tension to shear failure again in CT specimens under fatigue [19]. Additionally, the number of waveform counts after controlled drop of metal powder on a metal plate has been shown indicative to particle diameter [20].

It is therefore realized that the qualitative parameters of the received AE waveforms are useful for characterization of different material properties. As an arithmetic example from the above mentioned literature [10], oxide formation during corrosion in aluminum plates is related to high peak frequency of 477 kHz, while hydrogen evolution results in approximately 250 kHz and grain detachment in 110 kHz. On the other hand, grain detachment exhibits the highest absolute energy in the associated AE signals, more than 20 times higher than corresponding signals of oxide formation. The duration of the signals is also influenced from the source with grain detachment events resulting in the longest duration (122 μs), while oxide formation in just 11 μs. The rise time behaves in a similar way with values around 30% of the duration. As another example, shear crack propagation in thin aluminum plates under fatigue is escorted by *RA* values of 200 ms/V much higher than initial tensile cracking with 20 ms/V, while the RT undergoes an increase from less than 1 ms to more than 10 ms for the same shift in damage mechanism [19]. From these indicative examples, it is obvious that characterization schemes for metal materials and processes are based on AE shape parameters.

However, the specific values of the parameters derived in each case are very sensitive to the specific experimental set up and the general conditions like geometry. Therefore, comparisons should be very careful and only for exactly the same experimental conditions. This renders the results case-specific and not transferable to general models [21]. This is the reason that strict standardization has been applied to certain testing procedures [e.g. ASTM E569-07 for pressure vessels], while it is currently undertaken in other fields, like concrete [22], in order to limit the variability produced at least by different experimental conditions, like frequency sensitivity of the sensors.

Concerning all of the above studies and many more occupying with metals, the geometries of the specimens used for AE monitoring are mainly thin plates. It should be kept in mind that AE signals are elastic waves and therefore are subjected to attenuation as well as dispersion. In thin plates, propagation is by definition dispersive [23,24], due to the fact that different frequencies propagate on different phase velocities. This results in changes of the waveform shape as the pulse is propagating away from the source, meaning that if the source (crack) opens away from the receiver it will be recorded with a considerably different waveform than if it opens near the sensor. Therefore, the measured waveform parameters carry already the effect of dispersion corresponding to the actual propagation path. This effect can be quite strong as the distance between the source and the sensor increases, which is directly related to the sensor separation distance, especially for large structures like tanks or vessels [25,26]. It is understood that the location of the sensors relatively to the source is of primary importance. This is because, as shown by the examples above, criteria for crack classification or process characterization refer to the specific experimental conditions (including sensor separation distance). Thus, general application would not a priori lead to reliable results.

The present paper describes a numerical study simulating the propagation of an elastic wave through a homogeneous metal plate. The study does not focus on classic wave propagation features, like velocity and attenuation but mostly on the change of the AE waveform parameters, like duration, rise time, *RA*, central and peak frequency. The influence of propagation distance on these parameters is discussed, showing that the location of the events should be definitely taken into account for correct classification since some additional cm may well change the shape of the acquired waveform and consequently mislead the characterization of the material. The excited frequency is varied in order to examine different wavelengths as well as to resemble different resonance behavior of AE sensors from 100 kHz up to 2 MHz. This study aims to highlight the crucial influence of propagation distance on the AE wave, in order to increase the reliability of the characterization based on AE parameters. By knowing the dependence of specific waveform parameters on propagation distance through a certain material, it is possible to inversely calculate the original value of the parameter at the source and therefore, exclude the influence of dispersion which certainly masks some of the original information.

2. Numerical simulation

The fundamental equation governing the two-dimensional propagation of stress waves in an elastic medium, with viscous losses is as follows:

$$\rho\frac{\partial^2 u}{\partial t^2}=\left(\mu+\eta\frac{\partial}{\partial t}\right)\nabla^2 u+\left(\lambda+\mu+\xi\frac{\partial}{\partial t}+\frac{n}{3}\frac{\partial}{\partial t}\right)\nabla\nabla\cdot u \qquad (2)$$

where $u = u(x,y,t)$ is the time-varying displacement vector, ρ is the mass density, λ and μ are the first and second Lame constants, η and ξ are the first and second viscosities respectively, and t is time. The simulations were conducted using commercially available software [27,28]. It operates by solving Eq. (1) based on the method of finite differences with respect to the boundary conditions of the model, which include the input source that has pre-defined time-dependent displacement at a given location and a set of initial conditions.

The metal material was considered elastic without viscosity components. The numerical model consists of a homogeneous plate with properties of steel and specifically elasticity modulus, E of 210 GPa, Poisson's ratio 0.29 and density 7800 kg/m^3. These values lead to longitudinal and shear wave velocities of 5940 and 3230 m/s respectively. The thickness of the plate is 10 mm, its total length 500 mm, and twelve receivers were placed on the top surface with a separation distance of 40 mm. The receivers record the average of the vertical displacement of the nodes in their whole length. The excitation of 1 mm length was conducted at the bottom of the plate exactly below the first receiver, see Fig. 2. The excitation was one cycle while three different frequencies were applied, i.e. 100 kHz, 500 kHz and 2 MHz. This aimed at a variety of excited wavelengths and therefore, wave modes. Specifically for the 2 MHz, the wavelength is approximately 3 mm, which is shorter than the thickness of the plate. This may allow propagation of pure Rayleigh waves among the other wave modes. However, for the lowest frequency of 100 kHz, the wavelength is 60 mm, meaning that plate modes dominate, while Rayleigh cannot be formed. For

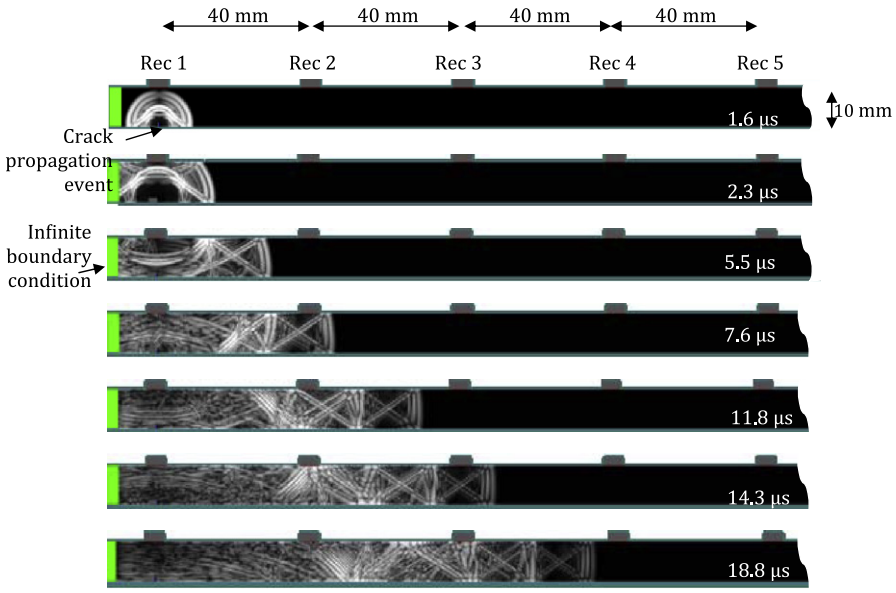

Fig. 2. A part of the geometrical model and consecutive displacement snapshots after excitation of one cycle of 2 MHz.

the intermediate case of 500 kHz, the wavelength is similar to the thickness.

In order for the simulation to produce reliable results, it is essential that certain guidelines are followed concerning mainly the spacing and time resolution of the wave equation solution. Convergence was checked in terms of spacing and time step resolution. In the present case the time step resolution for the calculations was 0.02108 μs. Considering the range of frequencies excited (from 100 kHz to 2 MHz) the basic period of the waves ranges between 0.5 to 10 μs. Even for the shortest period, each cycle is represented by approximately 23 points which is adequate for similar numerical studies [29]. The spacing resolution was set to 0.15 mm which is one twentieth of the wave length corresponding to the highest frequency of 2 MHz. Apart from the general rule of twenty points per wavelength [29], convergence was examined until the spacing resolution of 0.07 mm. With this fine resolution the transit time from the source to the last receiver was 74.56965 μs but the simulation time was quite long. The spacing resolution of 0.15 mm, which was selected, resulted in transit time of 74.5008 μs, being only 0.09% away but more than four times faster in calculation time. At the right and left ends of the beam, infinite boundary conditions were applied in order to avoid reflections. Fig. 2 shows consecutive snapshots of the displacement field for the case of 2 MHz. The wave propagates to the right reaching the successive transducers, while multiple reflections are noted moving between the top and bottom surface. As implied by a simple visual examination of the displacement fields, it would be very complicated to distinguish between different modes, except possibly the longitudinal wave which moves faster. The rest of the energy is divided to different modes and reflections making specific mode characterization troublesome. However, the wave parameters as measured from the AE point of view can be calculated, since the whole waveform is recorded. In practical AE measurements, the calculated signal duration is defined by certain settings applied by the user like the hit definition time (HDT), as well as the threshold and maximum duration. It is a certain fact that these settings influence the measured parameters, but the real time monitoring character of AE necessitates their use. These settings are selected based on experience according to the material and the expected values of the parameters. In the specific case, due to absence of noise, the onset of the waveform was defined by the first non zero point (zero-crossing), while the full duration of the simulated waveforms was 700 μs. At that point the signal has been attenuated to near zero level. The figures in the manuscript focus on the first part in order to show the meaningful part of the waveform, while calculations of AE parameters are made for the whole waveform.

3. Results

Fig. 3 shows the waveforms as captured by several receivers at different propagation distances. It is evident that the shape changes gradually; the receiver on top of the excitation exhibits its maximum voltage quite early, leading to very short RT and low *RA*. As the wave propagates, the waveform looses the initial strong peak, and the maximum peak is translated to later times, considerably increasing the RT and therefore, *RA* value.

Calculating the specific AE parameters of the waveforms recorded at the different sensors reveals that distance is a key factor for the AE measurements in plates. Fig. 4 shows the rise time vs. distance. RT starts at a very low value for the near-by sensor (approximately 10 μs), but almost monotonically increases as the wave propagates away and reaches the level of 70–100 μs for the furthest receiver at 440 mm, being increased by almost 10 times. The trend is similar for all frequencies, with the 2 MHz exhibiting slightly higher RT for long propagation.

Fig. 4b shows the dependence of peak amplitude, A on the traveling distance, normalized to the value of the first receiver for each frequency. The changes are also strong, following a certain decreasing trend. The peak amplitude finally decreases to 50% or less of the corresponding value measured by the first receiver. Again the strongest change (decrease) is exhibited by the highest frequency.

Since RT increases and A decreases, it is expected that the *RA* will exhibit an even stronger trend. This is shown in Fig. 5, where a strong increasing trend for any frequency is obvious. It is characteristic that for the excitation of 2 MHz, the original *RA* is 30 μs/V, while after 440 mm of propagation the *RA* of the same pulse is 1233 μs/V. These changes are crucial and certainly alter the original AE characteristics, as will also be discussed later.

Concerning frequency features, the central frequency (center of gravity of the FFT, as calculated by Eq. (1)) does not exhibit great fluctuations with distance. This means that the frequency content

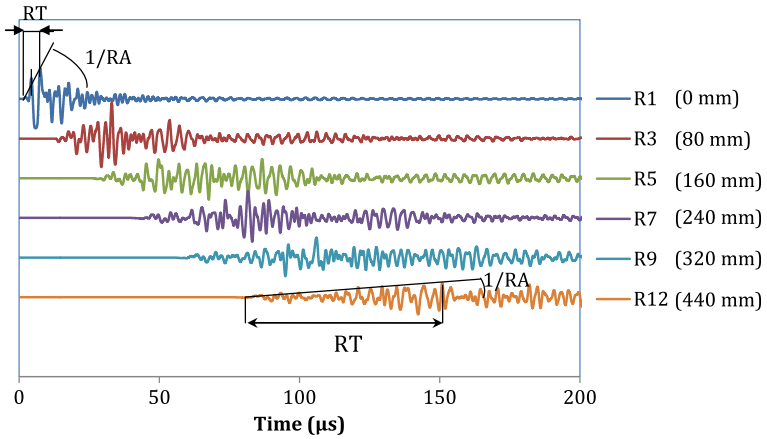

Fig. 3. Waveforms of different receivers after excitation of 1 cycle of 2 MHz in the geometric model of Fig. 2. In parentheses the horizontal distances of the receivers from the source.

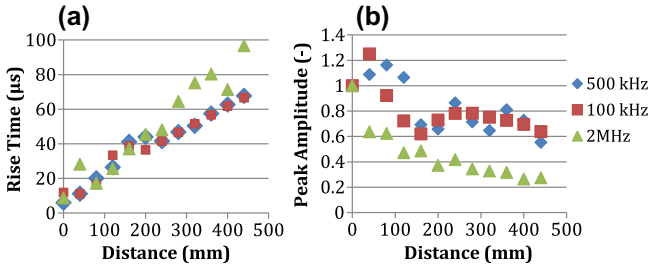

Fig. 4. (a) Rise time and (b) peak amplitude vs. distance for different excited frequency.

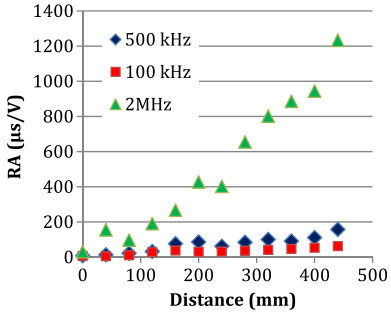

Fig. 5. *RA* value vs. distance for different frequency excitation.

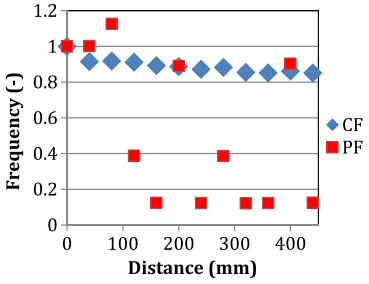

Fig. 6. Normalized central and peak frequency vs. distance for excitation of 2 MHz.

of the pulse changes only slightly (by about 15%), as indicatively seen in Fig. 6 for the excitation of 2 MHz. This is reasonable since no damping or scattering is present as an attenuation mechanism and although the wave energy is divided to several modes, the total pulse retains the original frequency content. However, the peak frequency, which depends only on the maximum magnitude of the spectrum exhibits intense fluctuations, especially at distances longer than 100 mm. It is indicative that in most cases of far away receivers, PF is of the order of 300 kHz, several times lower than the excited pulse. The PF seems indicative of the actual content of the pulse only for the three nearest receivers which are within 80 mm from the source. It is understandable that when monitoring AE with long separation between the sensors, it is mandatory to take into account the distance between the AE source and the receiver. If it is not taken into account, severe changes of up to 85% due to the distance would certainly mask the original PF (see again Fig. 6). On the other hand *CF* attains the original level for much longer propagation distance.

4. Discussion

As seen above, several AE parameters exhibit certain and mostly monotonic trends with distance. In general, the "dispersive" trends are similar for any excitation, but it should be pointed out that, as the original excitation frequency increases, the shift of AE parameters is stronger for the same distance. This could be connected to the transmitted modes, because as the frequency becomes higher, the short wavelength compared to the thickness allows for Rayleigh waves to be formed instead of plate waves. These changes in AE parameters owing to propagation may well mask possible changes due to the shift of fracture mode or change in the microstructural formation stage. From one of the experimental examples mentioned above, the transition between tension and shear as monitored during fatigue in aluminum plates is escorted by an *RA* increase of about 15 times (from approximately 10–20 ms/V at early fraction of fatigue life to almost 200 ms/V just before final failure, [19]). This was measured for rectangular plates of 60 mm, meaning that practically the distance between the crack tip and the sensors was limited to less than 40 mm. In case the distance is longer, that could be the case for a large tank bottom, the *RA* value may well suffer a change of more than 10 or even 40 times depending on the frequency of the event, as suggested in Fig. 5 for less than half a meter of propagation. Therefore, even if the AE signal belongs to a tensile event, it would certainly be misclassified to shear mode.

Concerning material corrosive processes, as monitored in [10], the oxide formation is related to the PF of 477 kHz, while hydrogen evolution exhibits 50% of this value and grain detachment PF decreased by 80%. However, the PF of a signal will suffer an extensive drop by more than 80% for propagation of 160 mm away from the

source, as suggested by the simulations and displayed in Fig. 6. Therefore, a signal from oxide formation after long propagation would be more likely misclassified as grain detachment using peak frequency criteria obtained from experiments on small laboratory specimens.

It is therefore, stressed out that any criteria concerning AE-based characterization should be escorted by a procedure that accounts for the propagating distance and clears the signal from the effect of dispersion. This will enable the correct classification of the AE signals as-emitted by the source (cracking or other process) and not the as-received by the sensor which already carries the distortion due to dispersive propagation. The first step of the correction is the numerical simulation to create the curves of the AE parameter of interest (e.g. *RA*) vs. the propagating distance for the corresponding thickness of the actual structure and different frequencies (or equivalently different values of wavelength/thickness, λ/h), see Fig. 7. The data of this figure come from Fig. 5 and are indicatively fitted by 2nd order polynomials, which yield high correlation coefficients, while exponential growth function would also be adequate. Consequently, for any received AE signal to be analyzed, based on its central frequency, the appropriate curve of (λ/h) is selected. The distance between the sensor and the AE source, which is automatically calculated by the location algorithm in all pieces of contemporary AE equipment, will directly indicate how much the *RA* has been shifted upwards and will provide a way to estimate the original value, near the source.

As a numerical example, consider an AE signal with *RA* = 500 μs/V and *CF* = 350 kHz, which is recorded 300 mm away from the source on a aluminum plate of $h = 3$ mm thickness. Using typical wave velocity of the material (6300 m/s), the wavelength λ is approximately 18 mm and therefore, $\lambda/h = 6$, see bottom solid line curve of Fig. 7. For the propagation distance of 300 mm, the *RA* is 6.1 times higher than the original as would be measured directly at the source. Therefore, the original *RA* equals 500/6.14 = 81.4 μs/V. This value, freed at least to a large extend from the effect of propagation distance through a thin plate, should be used for material characterization and not the one of the waveform captured at the sensor. If no correction is attempted, characterization should be limited to small size specimens or would lead to erroneous results and misclassification of the damage sources.

In the above discussion, the influence of propagation distance is studied for a 1 mm crack, breaking the bottom surface of the plate (the sensors being at the top surface). The depth to the crack has been shown to substantially influence the magnitude proportions of the symmetric and antisymmetric modes in aluminum plates [26]. In order to check the effect of the depth of the crack on conventional AE parameters, simulations were repeated for two additional depths to crack and the frequency of 500 kHz. Specifically, the crack was located at the middle of the plate (crack from 4.5–5.5 mm) in one case and at the top (0–1 mm) in the other.

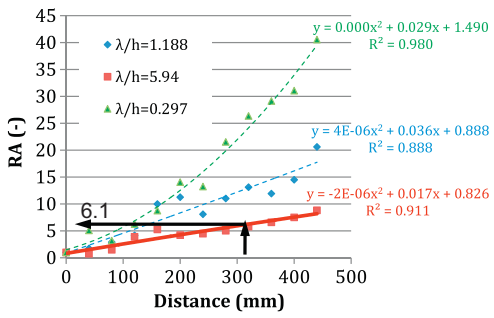

Fig. 7. Normalized *RA* value vs. distance for different wavelength to thickness ratios (λ/h).

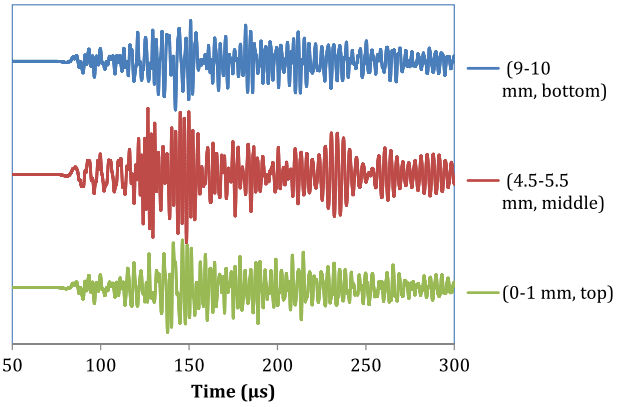

Fig. 8. Waveforms collected from receiver 12 (440 mm from the source) after excitation of 1 cycle of 500 kHz for three different depths to crack. In parentheses the start and end points of the vertical crack in the thickness of 10 mm.

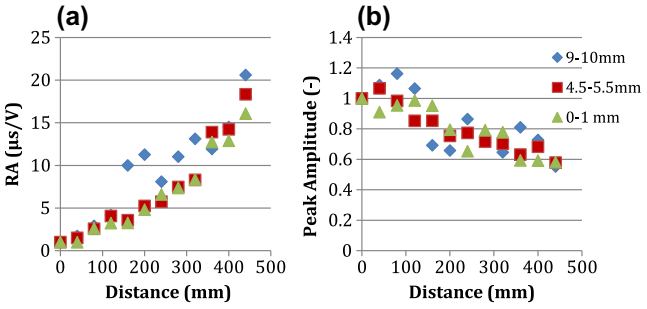

Fig. 9. (a) *RA* and (b) peak amplitude vs. distance for different depths to crack and frequency of 500 kHz.

Waveforms collected at the last receiver (R12) are shown in Fig. 8 for the three cases of the depth to crack. Though certain differences are visible in the waveform shape, results concerning conventional AE parameters for the three different depths to crack exhibit a very similar behavior, as shown in Fig. 9. This figure indicatively includes *RA* (Fig. 9a) and peak amplitude (Fig. 9b). It seems that for a crack of size one tenth of the plate thickness the depth is not of primary importance as to the conventional AE parameters. It is therefore implied that the inversion procedure for correction of the waveform features can be applied regardless of the depth to crack in thin metal plates since despite differences in waveform shape, the basic AE parameters behave very similarly.

5. Conclusions

This paper presents a numerical study of wave propagation in a thin homogeneous plate. The novelty of the study is the focus on distortion of waveform parameters that are important from the acoustic emission point of view and not classical wave parameters like velocity and attenuation. Propagation at different distances exercises strong influence on the shape of the pulse, changing critically waveform parameters, like rise time, amplitude, *RA*, peak frequency. The goal of the work is twofold; to highlight the issue of propagation distance influence in quantitative AE testing in thin structures and consequently to propose the way to inversely "correct" the AE values. This can be achieved by combining the knowledge of the location of the AE events, which is a standard feature available in all contemporary AE pieces of equipment with the numerically obtained functions between the AE parameters and distance. The correction should be taken into account for AE-based classification of active sources, since most of the criteria

established for material characterization so far do not account for the dispersive effect of plate geometry. The research should proceed in joint numerical and experimental studies, using also curved geometries, as well as three dimensional simulations which would better represent the actual geometries and incorporate viscosity components, which although weak in metals, may have an effect after long propagation.

References

[1] Kaiser J. Results and Conclusions from Measurements of Sound in Metallic Materials under Tensile Stress, PhD Thesis, 1950.Technische Hochshule Munich.

[2] Grosse CU, Ohtsu M. Acoustic emission testing, Springer, 2008. Heidelberg.

[3] Shiotani T, Bisschop J, Van Mier JGM. Temporal and spatial development of drying shrinkage cracking in cement-based materials. Eng. Fract. Mech. 2003;70(12):1509–25.

[4] Grosse C, Reinhardt H, Dahm T. Localization and classification of fracture types in concrete with quantitative acoustic emission measurement techniques. NDT Int 1997;30(4):223–30.

[5] Aggelis DG, Shiotani T, Terazawa M. Assessment of construction joint effect in full-scale concrete beams by acoustic emission activity. Eng Mech 2010;136(7):906–12.

[6] Ono K. Structural integrity evaluation using acoustic emission. J Acoustic Emission 2007;25:1–20.

[7] Aggelis DG. Classification of cracking mode in concrete by acoustic emission parameters. Mech Res Comm 2011;38:153–7.

[8] De Oliveira R, Marques AT. Health monitoring of FRP using acoustic emission and artificial neural networks. Comput Struct 2008;86:367–73.

[9] Overgaard LCT, Lund E, Camanho PP. A methodology for the structural analysis of composite wind turbine blades under geometric and material induced instabilities. Comput Struct 2010;88:1092–109.

[10] Boinet M, Bernard J, Chatenet M, Dalard F, Maximovitch S. Understanding aluminum behaviour in aqueous alkaline solution using coupled techniques. Part II: acoustic emission study. Electrochim Acta 2010;55:3454–63.

[11] Amami S, Lemaitre C, Laksimi A, Benmedakhene S. Characterization by acoustic emission and electrochemical impedance spectroscopy of the cathodic disbonding of Zn coating. Corrosion Sci 2010;52:1705–10.

[12] Clough RB, McDonough WG. The measurement of fiber strength parameters in fragmentation tests by using acoustic emission. Composites Science and Technology 1996;56:1119–27.

[13] Yonezu A, Arino M, Kondo T, Hirakata H, Minoshima K. On hydrogen induced Vickers indentation cracking in high-strength steel. Mech Res Comm 2010;37:230–4.

[14] Brown JA, Vendra LJ, Rabiei A. Bending properties of Al–steel and steel–steel composite metal foams. Metall Mater Trans A 2010;41(11):2784–93.

[15] Trojanová Z, Száraz Z, Chmelíka F, Lukác P. Acoustic emission from deformed Mg–Y–Nd alloy and this alloy reinforced with SiC particles. J Alloys Compounds 2010;504(2):L28–30.

[16] Dang Hoang T, Herbelot C, Imad A. Rupture and damage mechanism analysis of a bolted assembly using coupling techniques between A.E. and D.I.C., Eng Struct. 2010;32(9):2793–2803.

[17] Jin Z, Gong B, Jin W, Wen B. Analysis of Acoustic Emission Signals from stainless Steel with Different Wavelet Bases, In: 2008 IEEE International Symposium on Knowledge Acquisition and Modeling Workshop Proceedings, KAM 2008, art. no. 4810635, p. 892–895.

[18] Roberts TM, Talebzadeh M. Acoustic emission monitoring of fatigue crack propagation. J Construct Steel Res 2003;59:695–712.

[19] Aggelis DG, Kordatos EZ, Matikas TE. Acoustic emission for fatigue damage characterization in metal plates. Mech Res Comm 2011;38:106–10.

[20] Boschetto A, Quadrini F. Powder size measurement by acoustic emission. Measurement 2011;44:290–7.

[21] Scholey JJ, Wilcox PD, Wisnom MR, Friswell MI. Quantitative experimental measurements of matrix cracking and delamination using acoustic emission. Compos A 2010;41:612–23.

[22] Ohtsu M. (Chairman). Recommendations of RILEM Technical Committee 212-ACD: acoustic emission and related NDE techniques for crack detec- tion and damage evaluation in concrete: 3. Test method for classification of active cracks in concrete structures by acoustic emission. Mater Struct 2010;43(9):1187–9.

[23] Rose J. Waves in plates, in "Ultrasonic waves in solid media", 1999, Cambridge University Press.

[24] Brepta R, Vales F, Cerv J, Tikal B. Rayleigh wave dispersion due to spatial (FEM) discretization of a thin elastic solid having non-curved boundary. Comput Struct 1996;58(6):1233–44.

[25] Anastasopoulos A, Kourousis D, Botten S, Wang G. Acoustic emission monitoring for detecting structural defects in vessels and offshore structures. Ships Offshore Struct 2009;4(4):363–72.

[26] Hamstad MA, O'Gallagher A, Gary J. A wavelet transform applied to acoustic emission signals: part 1: source identification. J Acoustic Emission 2002;20:39–61.

[27] Wave2000, Cyber-Logic, Inc., NY. <http://www.cyberlogic.org>.

[28] Kaufman JJ, Luo G, Siffert RS. Ultrasound simulation in bone. IEEE Trans Ultrason Ferroelect Frequency Control 2008;55(6):1205–18.

[29] Moser F, Jacobs LJ, Qu J. Modeling elastic wave propagation in waveguides with finite element method. NDT&E Int 1999;32:225–34.